

Chapter 4

Multi-PON access network using coarse AWG

This chapter provides a detailed analysis of the AWG routing performance to integrate multiple physical PON locations in an access network, where the main features and performance of which are presented and evaluated. To that extent, centralised wavelength allocation by means of a single, coarse AWG-based, OLT, is displayed to demonstrate network transparency in view of the fact that network ONUs can be accessed by multiple wavelengths. The bidirectional transmission of wavelengths through the single AWG network device in the OLT has been simulated for both the flat-top and Gaussian AWG models with the intention of establishing a valid comparison of the contribution of PDW shift in successful network routing. Subsequently, network grooming operational figures are presented, based in the performance of only the Gaussian device due to their extensive research development and drive to become commercially-available in the near future.

4.1 Simulated access network architecture

The focus of the proposed work is to capture the merits of time and wavelength multiplexing in a new access network architecture [1] encapsulating scalability and interoperability of TDM and WDM-PONs, to grant smooth upgrade from standard to next generation access networks. This is achieved by utilising CWDM [2, 3] to route multiple physical PON locations to a common OLT. Hence the network will exhibit centralised wavelength assignment to manage network resources across multiple physical PONs according to traffic penetration and requirement in bandwidth. The network architecture, shown in Figure 4-1, exhibits a single 4×4 coarse AWG

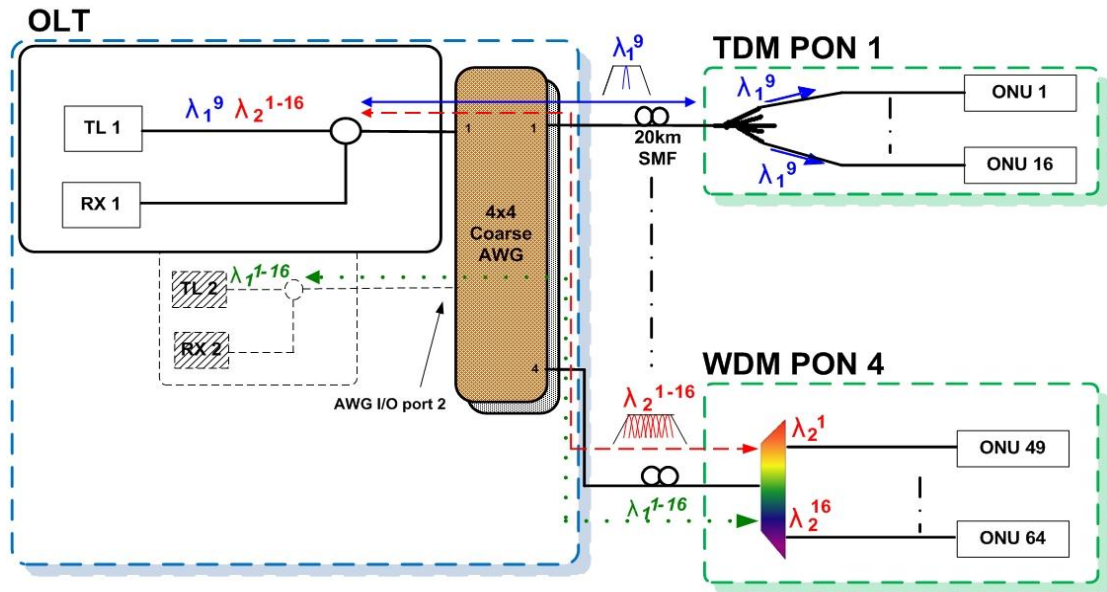


Figure 4-1 Multi-PON network architecture

in the OLT, to route multiple TDM and WDM-PONs by means of a single tunable laser (TL1) and receiver (RX1). The coarse AWG 7 nm, 3 dB Gaussian passband windows [3] are denoted in Figure 4-1 by coarse ITU-T channels $\lambda_1=1530$ nm and $\lambda_2=1550$ nm, set to accommodate in the simulation setup up to 16, 0.4 nm-spaced wavelengths to address a total of 16 ONUs per PON. This is illustrated in Table 4-1 where each row represents a coarse channel, populated by 16, 0.4 nm spaced wavelengths. Future development can utilise smaller wavelength spacing, e.g. 0.2 nm, to scale up the number of ONUs of a PON to 32, allowing for extended network penetration. In a PON level, increasing the number of PONs can be achieved by employing an AWG with greater number of I/O ports.

Table 4-1 Coarse and fine wavelengths allocation

Coarse Ch \ fine λ	fine λ															
	1	2	3	4	...	13	14	15	16							
$\lambda_1 = 1530$ nm	λ_1^1	λ_1^2	λ_1^3	λ_1^4	...	λ_1^{13}	λ_1^{14}	λ_1^{15}	λ_1^{16}							
$\lambda_2 = 1550$ nm	λ_2^1	λ_2^2	λ_2^3	λ_2^4	...	λ_2^{13}	λ_2^{14}	λ_2^{15}	λ_2^{16}							
$\lambda_3 = 1570$ nm	λ_3^1	λ_3^2	λ_3^3	λ_3^4	...	λ_3^{13}	λ_3^{14}	λ_3^{15}	λ_3^{16}							
$\lambda_4 = 1590$ nm	λ_4^1	λ_4^2	λ_4^3	λ_4^4	...	λ_4^{13}	λ_4^{14}	λ_4^{15}	λ_4^{16}							

In downstream, TL1 will utilise λ_1^9 , placed at the centre of the AWG coarse channel λ_1 , to broadcast information to all ONUs of TDM-PON1. To address a WDM-PON, TL1 will sequentially switch on all 16 wavelengths, centred ± 3.2 nm around coarse channel λ_2 , to address jointly all ONUs in WDM-PON4.

The interoperability of TDM and WDM-PONs is a key feature of the architecture since, unlike previous proposals [4, 5], it allows smooth migration to multi-wavelength optical access by substituting the splitter in the distribution point with a multiplexing unit, justifying parallel operation of TDM and WDM-PONs to address bandwidth requirements from subscribers with different service levels more effectively.

In the ONU, reflective semiconductor optical amplifiers (RSOAs) are intended to be integrated to implement colourless transceivers, as it will be extensively described in chapter 5, thus no modification in customer premises equipment will be required in the migration from TDM to WDM. As it will be demonstrated in chapter 5, this will allow for all ONUs that are served downstream by a single transmitter in the OLT, e.g. TL1, to be terminated upstream to a common receiver, e.g. RX1, connected to the same AWG port of TL1, by means of the AWG's reciprocal characteristic [6].

The network is highly scalable since extra tunable lasers can be easily incorporated at unused AWG ports in the OLT to increase bandwidth provision at high traffic load. As shown in Figure 4-1, TL1 uses 16, 0.4 nm-spaced wavelengths λ_2^{1-16} , positioned within coarse channel λ_2 , to address all ONUs of WDM-PON4. In case the total bandwidth demand cannot be met by TL1 alone, TL2 will be connected to the second AWG port to share the load using the Latin-routing property of the AWG [6]. TL2 could utilise another 16 wavelengths, this time

positioned within the passband of coarse channel λ_1 to also address all ONUs of WDM-PON4, consequently providing each PON with multiple wavelengths concurrently to accommodate on-demand bandwidth allocation [7]. This is possible since multiple FSRs of a simple 1×16 AWG in the distribution point are used to accommodate all coarse channels and an algorithm preventing two TLs addressing the same ONU simultaneously.

Finally, the ratio of subscriber number to OLT transmitters and receivers in the network is fairly high, allowing for low inventory count in the OLT. As shown in Figure 4-1, all ONUs served by TL1 will be terminated to a single receiver, RX1.

4.2 VPI network elements

The physical layer network model and individual elements were devised using the VPI physical layer simulation platform. Subsequently, the functional blocks and design parameters for the OLT, outside plant and ONU, as well as their corresponding modules are described, and successively evaluated independently and in the network as a whole.

4.2.1 Optical line terminal

The OLT block diagram, shown in Figure 4-2(a), is displayed in conjunction with its corresponding VPI model shown Figure 4-2(b). In downstream, TL1 is realised by an external modulated distributed feedback (DFB) laser module, by means of a standard Mach-Zehnder modulator (MZM) and pseudo-random bit sequence (PRBS) generator applied at the MZM's radio frequency (RF) input. The external modulated DFB laser output port is applied at an optical attenuator to model the loss associated with the MZM which is not accounted in the standard VPI module. The output port of the attenuator is connected to a 3-port optical circulator to allow bidirectional transmission and via the coarse AWG, simulated using the 5×5 Gaussian AWG device [3], to the output of the OLT. In upstream, an identical AWG is used since VPI does not support bidirectional transmission in the majority of its standard modules.

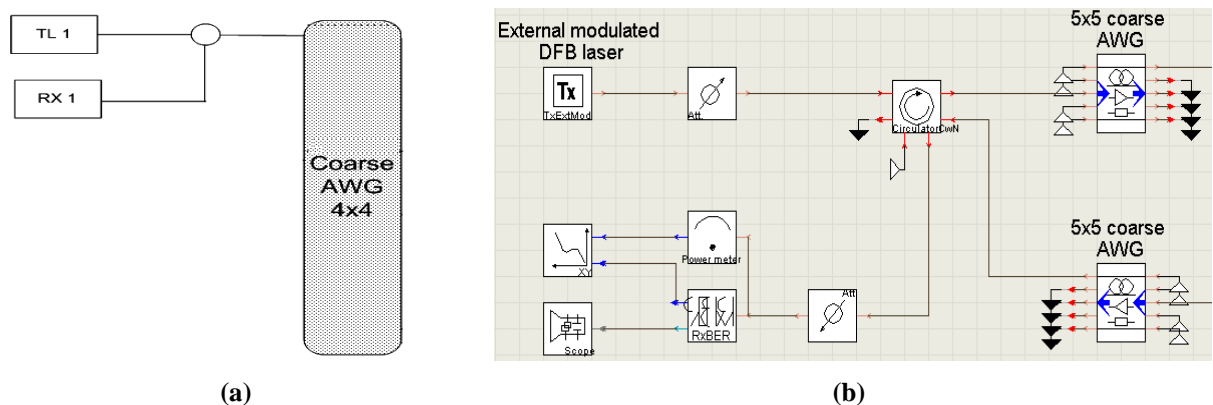


Figure 4-2 Optical line terminal modelling

Following the AWG upstream, the circulator output is directly applied at an optical attenuator, this time used to obtain bit-error-rate (BER) performance characteristics, subsequently connected to an RxBER module employing an avalanche photodetector (APD) and BER measurement unit. Consequently, the error-rate and detected signal outputs of the RxBER are applied at the corresponding inputs of an XY-plot module y-axis and scope, to obtain BER performance characteristics and display eye diagrams respectively. Finally, the optical power at the output of the RxBER module is measured using an optical power meter that is subsequently applied at the XY-plot module x-axis input to obtain also BER performance characteristics.

VPI Table 4-2 includes the modelling parameters of the external modulated DFB laser module. As denoted in the table, first part represents the DFB laser emission parameters corresponding to the emission frequency (wavelength), average emitted power level in milli-Watt units and laser typical linewidth of 5 MHz [8]. Second part represents the downstream data configuration for which a PRBS order of 7, corresponding to a length of 2^7-1 , was employed at 2.5 Gbit/s to comply with standard PON data rates [9-12], determined by a simulation global parameter BitRateDefault. The third part represents the MZM parameters utilising extinction ratio (ER) of 20 dB and symmetry factor of -0.176, corresponding to an alpha factor of 0.7 to match typical specification of a commercially-available device [13]. The parameters laser azimuth and ellipticity are used to adjust the downstream signal state of polarisation (SOP) in order to engage the transmission via either the TE or TM passband of the AWG.

Table 4-2 OLT transmitter modelling parameters

-	f	SampleRate	SampleRateDefault	Hz
-	f	BitRate	BitRateDefault	bit/s
-	f	Laser_EmissionFrequency	2.9979e8/1550.12e-9	Hz
1	f	Laser_AveragePower	1.6e-3	W
-	f	Laser_Linewidth	5e6	Hz
-	f	RiseTime	1.0/4.0/BitRateDefault	s
-	i	PreSpaces	0	
2	i	PostSpaces	0	
-	i	PRBS_Type	PRBS_N	
-	f	MarkProbability	0.5	
-	i	PRBS_Order	7	
-	i	MarkNumber	7	
-	i	PRBS_CodeWord		
-	i	PRBS_InputFilename		
-	f	Laser_Azimuth	0	deg
-	f	Laser_Ellipticity	0	deg
3	f	Laser_InitialPhase	0	deg
-	f	ModulatorMZ_ExtinctionRatio	20.0	dB
-	f	ModulatorMZ_SymmetryFactor	-0.176*1 # alpha factor 0.7	
-	i	ModulatorMZ_ChirpSign	Positive	

VPI Table 4-3 includes the two modelling parameters used in the 3-port optical circulator. The insertion loss of the module is set to typical 1 dB for clock-wise direction and rejection loss of typical 40 dB in the anti clock-wise direction [14], to prevent leakage of the transmitter downstream signal into the receiver path.

Table 4-3 3-port optical circulator modelling parameters

f	InsertionLoss	1	dB
f	Rejection	40	dB

VPI Table 4-4 includes the modelling parameters of the optical receiver RX1, employing an APD. Initially, the parameters responsivity and avalanche multiplication were set according to a commercially-available JDSU ERM577 receiver [15], operating at 2.5 Gbit/s with sensitivity of -33 dBm at 10^{-9} BER. To consider the worst case, the detector avalanche multiplication was set to 4 in order to allow sensitivity of -30 dBm at 10^{-9} BER. In addition, to operate at 2.5 Gbit/s, the electrical bandwidth of the receiver post-detection low-pass filter (LPF) was set to 1.875 GHz corresponding to $0.7 \times$ bit-rate required for non-return-to-zero (NRZ) encoding [16].

Table 4-4 Optical receiver RX1 modelling parameters

ResponsivityDescripti	ResponsivityParameter	
f	Responsivity	0.7 A/W
ResponsivityFilename		
PhotodiodeModel	APD	
f	DarkCurrent	0.0 A
f	DarkCurrentMultiplied	0.0 A
f	DarkCurrentNonMultip	10e-9 A
f	AvalancheMultiplicatio	4
f	IonizationCoefficient	1.0
f	ThermalNoise	10e-12 A/Hz ^(1/2)
ShotNoise	On	
BackEnd	On	
f	Gain_BE	1
FilterType_BE	LowPass	
f	A	
f	B	1. -1.
TransferFunction_BE	Bessel	
f	Bandwidth_BE	0.75* 2.5e9 Hz

4.2.2 Optical network unit

The devised ONU shown in Figure 4-3 is relatively straightforward at this stage since it is realised by an externally modulated DFB laser and APD of similar specifications to their OLT counterparts. The ONU design will be considerably complicated with the inclusion of an RSOA to enhance network dynamicity as will be analysed in the following chapter. In contrast, the ONU design presented here is adequate for the purpose of critically establishing multiple PON operation through the AWG.

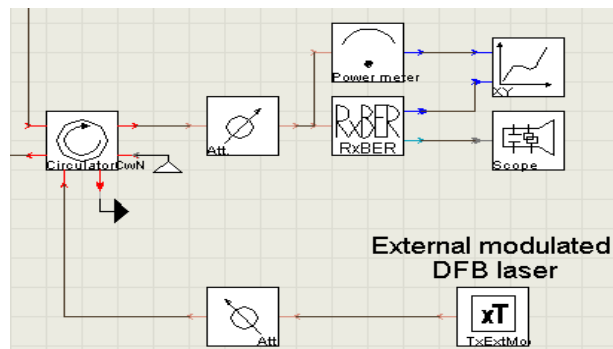


Figure 4-3 Optical network unit modelling

4.2.3 Outside plant simulation

The outside plant block diagram, shown in Figure 4-4(a), is displayed in conjunction with the VPI model, shown in Figure 4-4(b). The 20 km SSMF is modelled using a standard universal fibre VPI module, featuring bidirectional signal flow, Rayleigh and Brillouin backscattering, nonlinearities, various dispersion effects and loss [17]. Subsequently, two 1×16 multiplexers are employed using standard $1 \times N$ AWG modules to allow bidirectional transmission that is not supported in a single module in VPI as already indicated.

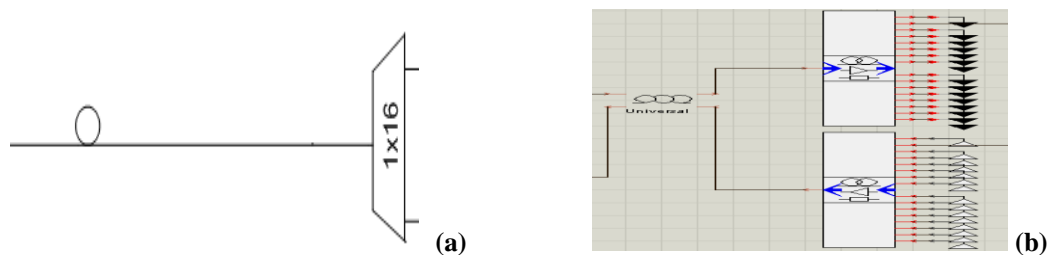


Figure 4-4 Outside plant modelling

VPI Table 4-5 includes the modelling parameters for the 20 km SSMF, particularly accounting for Rayleigh backscattering, crucially important when bidirectional transmission will be considered through a single fibre with RSOAs employed in each ONU. To form a typical Rayleigh backscattering reference power level of -35 dB in a 20 km SSMF at 1550 nm [18], the Rayleigh backscattering coefficient and the effective group index were employed [19] as shown in the table. Finally, a default PMD coefficient of 0.1 ps/ $\sqrt{\text{km}}$ was utilised to represent a typical fibre [19].

Table 4-5 20 km single mode fibre modelling parameters

[-] i	NumberOfFiberSpan	1	
[-] f	Length	20.0e3	m
[-] [f]	AttenuationDescriptio	AttenuationParameter	
[-] f	Attenuation	0.2e-3	dB/m
[-] [f]	AttFilename		
[-] f	ReferenceFrequency	193.1e12	Hz
[-] [f]	DispersionDescriptio	DispersionParameters	
[-] f	Dispersion	16e-6	s/m ²
[-] f	DispersionSlope	0.08e3	s/m ³
[-] [f]	DispersionFilename		
[-] f	PMDCoefficient	0.1e-12/31.62	s/sqrt(m)
[-] f	CorrelationLength	50.0	m
[+] [f]	Nonlinear Effects		
[-] [f]	RayleighScattering	Yes	
[+] [f]	Rayleigh Scatteri		
[-] [f]	Backscatter Descri	OTDR	
[-] f	EffectiveGroupInd	1.47	
[-] f	OTDRPulseWidth	1e-9	s
[-] [f]	Rayleigh Descriptio	RayleighCoefficient	
[-] f	RayleighBackscat	-80.0	dB 1/m
[-] [f]	RayleighFilename		

With reference to typical architectures [20-23], the distribution point to simulate a WDM-PON comprising a 1×16 multiplexer, is shown in VPI Table 4-6, as opposed to a simple 1:16 splitter to provide downstream broadcasting in typical TDM-PONs. In the case of the former, a standard VPI de/multiplexer unit based on physical parameters of a prototype device [24] was employed with the exception of manipulating the insertion loss figure at centre wavelength to a value of 4 dB to match practical devices [25].

Table 4-6 Distribution point multiplexer modelling parameters

[-] f	CenterFrequency	193.375e12 #1550.32e-9	Hz
[-] f	LossAtCenterFreque	4	dB
[-] f	FreeSpectralRange	16*50e9	Hz
[-] f	ChannelSpacing	50.0e9	Hz
[-] i	NumberOfChannels	16	
[-] f	WaveguideWidth	7.5e-6	m
[-] f	SlabModeIndex	1.5019	
[-] f	NormalizedPropCons	0.52	
[-] f	InputOutputWavegui	11.0e-6	m
[-] f	ArrayedWaveguides	1.7e-6	m
[-] f	RandomPhaseNoise	100	deg

4.3 Network routing and simulation results

The physical layer simulation testbed, shown in Figure 4-5, was initially devised to model the bidirectional routing performance of the Gaussian AWG. In particular it was used to demonstrate the network's capability to serve all ONUs comprising two physical PONs applied at the AWG I/O ports 4 (WDM-PON4) and 3 (WDM-PON3) via coarse channels of the device. Two WDM-PONs were simulated in order to monitor the collective routing of multiple wavelengths of each physical PON location through coarse passbands, and in that direction to evaluate the crosstalk for the wavelengths positioned in the passband edges.

As shown in Figure 4-5, in the system ONU a 2^7-1 PRBS at 2.5 Gbit/s, to reduce simulation time, was applied at a MZM's RF input to externally modulate a DFB laser at 2 dBm for upstream transmission with a safety margin of 3 dB. Externally modulated lasers were used instead of RSOAs at this stage of experimentations, purely for the purpose of demonstrating the AWG routing capabilities. In WDM-PON3 and WDM-PON4 the modulated 50 GHz, ITU-T wavelengths λ_2^{1-16} and λ_1^{1-16} , representing each of the 32 ONUs in total among the two PONs, ranging from 1553.33 nm to 1547.32 nm and 1533.47 nm to 1552.60 nm respectively, were applied to the corresponding circulator to allow bi-directional transmission and via the individual 1×16 multiplexers and 20 km SSMFs transmitted to the designated AWG router inputs in the OLT to be routed to a common AWG output by means of the nominated coarse passbands denoted by λ_2 and λ_1 . Prior to reception by a single broadband APD [26] of all upstream ONUs through a single AWG port achievable due to the grooming and Latin-routing [6] properties of the AWG, another circulator was used in the OLT to separate upstream and downstream transmission. Unused AWG output ports upstream can be employed to increase network penetration by allowing either additional PONs or ONUs within existing PONs to be

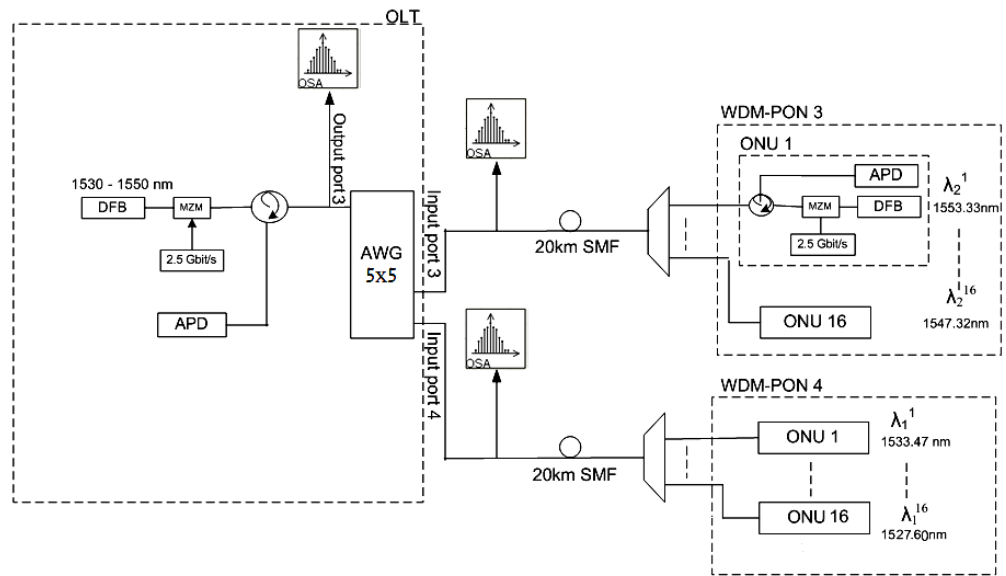


Figure 4-5 Physical layer simulation testbed

served via extra individual APD receivers and corresponding TLs. The number of individual transceivers depends on the total number of ONUs and the bandwidth distribution among the TLs.

In downstream, a random sequence source in the OLT of similar specifications to the one used upstream was employed to externally modulate a DFB laser as shown in Figure 4-5. Wavelengths around coarse channels at 1530 nm and 1550 nm were utilised to address WDM-PON4 and WDM-PON3 respectively. Adjacent channels were chosen in order to investigate and evaluate potential figures of channel crosstalk in the coarse AWG following the exact equivalent processing mechanism to transmit wavelengths as described for upstream. Following distribution, data destined to each ONU was terminated in individual APD receivers.

To demonstrate collective upstream routing at PON level, allowing the provision of just a single AWG output for all ONUs connected to more than one PON, three wavelengths were activated in each PON3 and PON4. Figure 4-6 shows the VPI spectra at AWG input ports 3 and 4 and corresponding output port 3. It can be observed that although all upstream wavelengths from PON3 are applied to input port 3 and those of PON4 to input port 4, they are all routed through their corresponding AWG coarse channels to a common destination, demonstrating the potential of the proposed architecture to handle multiple PONs through single ports of its passive router concurrently [27].

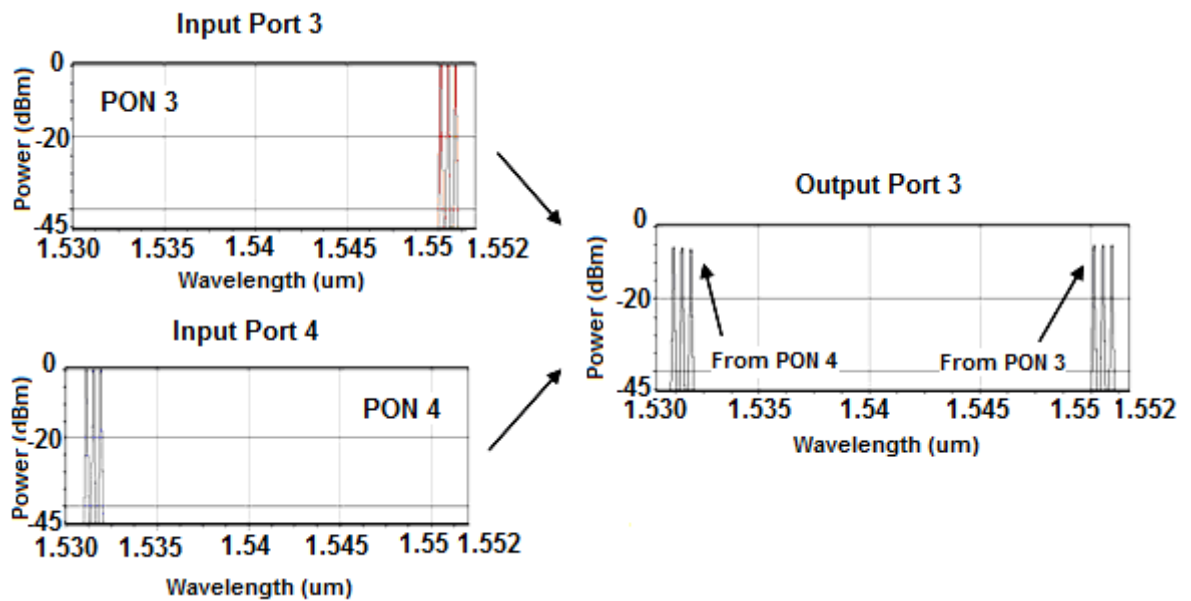


Figure 4-6 AWG input and output ports upstream spectra [27]

Alternatively, to monitor downstream performance, Figure 4-7 displays the spectrum plots of the AWG input port 3 and corresponding output ports 3 and 4. Simulation results signify that downstream wavelengths at the OLT applied sequentially at port 3, however displayed here simultaneously, are successfully routed in groups by means of their assigned AWG coarse channels to the designated outputs according to PON3 and PON4 physical termination.

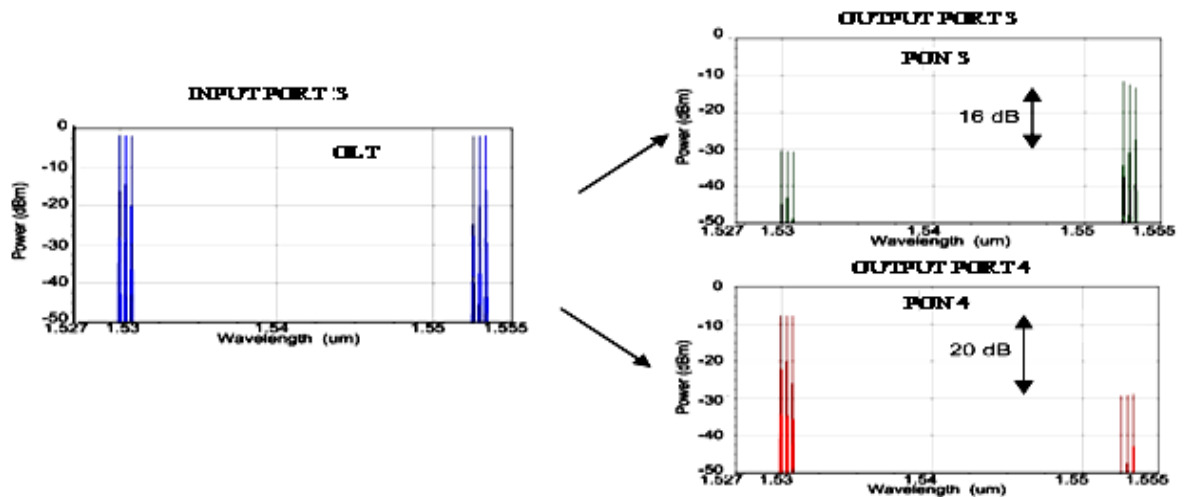


Figure 4-7 AWG input and output ports downstream spectra

Also present in the figure, is a representation of crosstalk isolation between adjacent coarse passbands. To evaluate this, the three longest wavelengths λ_2^{1-3} of coarse channel λ_2 , representing ONUs in PON3, and the three wavelengths λ_1^{8-10} located at the centre of coarse channel λ_1 , representing ONUs in PON4, were deliberately employed to account for varying transmission losses due to the AWG Gaussian response passbands and their contribution to crosstalk. As indicated in Figure 4-7, output port 3 spectra demonstrates the worst case crosstalk isolation of around 16 dB due to the higher attenuation of useful wavelengths at the passband edges of the AWG, representing potential ONUs of a WDM-PON. This relatively low figure is however further compensated by an extra isolation of successive network elements in a WDM-PON. In contrast, output port 4 spectra demonstrates increased crosstalk isolation of 20 dB, as a consequence of reduced attenuation of valuable wavelengths at the passband centre, where an individual wavelength could be used to serve ONUs of a TDM-PON.

4.4 Coarse-fine grooming in the presence of passband shifting

Section 3.3 in the previous chapter described the development of the Gaussian and flat-top response AWG models and the mapping characteristics of multiple 50 GHz spaced wavelengths to determine each AWG passband capacity in ONU penetration and evaluate wavelength power distribution. Further investigations into the efficient routing performance of the stricter specification Gaussian and flat-top AWGs, when integrated in a network to bidirectionally distribute ONUs, presented in preceding sections, have not taken into consideration the very critical PDW shift and associated PDL of the specified AWGs. PDW is known to impose a restriction in multi-wavelength operation of wide passband AWGs and therefore to limit the routing performance of the network [3]. To perform simulations for the worst case scenario, PDW shifts of up to 1.8 nm at room temperature [3] were considered in the model. Device thermal stability was not taken into consideration since in the proposed topology the AWG is placed at the OLT and consequently it is assumed to operate at room temperature.

Figure 4-8 displays simulation results of measured PDL versus operating wavelength for both profile AWGs at PDW shifts of 0 nm, 1.5 nm and 1.8 nm using the Mueller technique [28], the most effective mean of evaluating PDL of a passive device by calculating minimum and maximum output power levels ratio when its input is exposed to a set of determined SOPs (see appendix A for mathematical modelling). The vertical lines in the figure represent the ± 3.2 nm spectral width required for transmission of all wavelengths in a PON. As becomes evident from the figure, the PDL varies from 0 dB at centre wavelength to more than 5 dB outside the transmission band. As expected, the 0 nm shift curve for the Gaussian response exhibits insignificant residual PDL due to the random phase errors in the AWG VPI modules. On the contrary, the PDL for the 1.5 nm and 1.8 nm curves demonstrates asymmetric, linearly increasing loss with regard to the centre wavelength at $\lambda_2^9 = 1550.12$ nm since, due to shifting,

the longer wavelengths suffer extended PDL. It can be further observed that the longest wavelength in the passband, at $\lambda_2^1=1553.33$ nm, experiences the highest PDL with approximately 2.5 dB more loss than the central wavelength. In the case for the flat response, the PDL for the 1.5 nm and 1.8 nm curves demonstrates a 0 dB figure for most of the transmission band and reaches to its maximum of 2.5 dB for 1.8 nm shifting. In addition, since the PDL for 0 nm shift demonstrated 0 dB figure across the entire transmission passband, it was not displayed in the figure. Finally, it can be further observed that the spectral width available for transmission decreases with the increasing of the shifting, and so, according to acceptable PDL of 3 dB, the maximum shifting in the Gaussian channel for error free transmission is 1.8 nm.

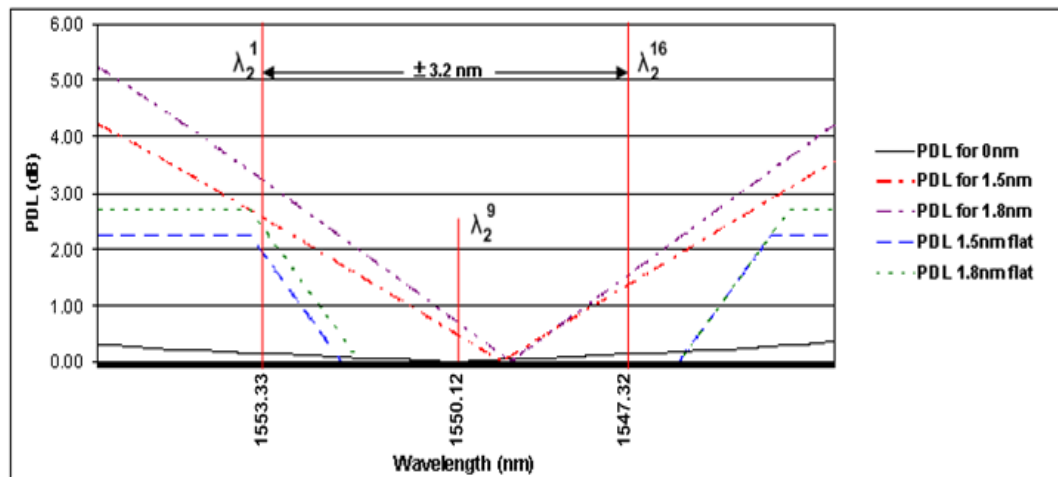


Figure 4-8 Polarisation-dependent loss vs. operating wavelength for flat and Gaussian channels

Phase errors in the AWG can also contribute towards the rise of PDL. Although typical phase errors of approximately 108° have been reported in literature [29] assuming 30 mm waveguide lengths of the prototype Gaussian AWG [3], a worst case 270° phase error was employed in the devised AWG following the advice of a major photonic devices vendor [30].

To demonstrate the effect of wavelength shift and loss superimposed at the transmitted wavelengths, Figure 4-9(a) and Figure 4-10(a), corresponding to the flat-top and Gaussian passbands, display the PDW shift of the central channel at $\lambda_2=1550$ nm for which the TM response is -1.8 nm shifted with respect to the TE. Figure 4-9(b) and Figure 4-10(b) display the resulting passband, where all 16 wavelengths are linearly vertically polarised and consequently routed via the TM response solely. As becomes evident from Figure 4-9(b), except for the 5 dB channel insertion loss of the flat response, the longest wavelength at $\lambda_2^1=1553.33$ nm suffers an additional 2.5 dB loss compared to the central wavelength at $\lambda_2^9=1550.12$ nm due to the increase of PDL. In the case for the Gaussian response in Figure 4-10(b), as opposed to the central wavelength at $\lambda_2^9=1550.12$ nm, the longest wavelength at $\lambda_2^1=1553.33$ nm suffers an additional loss of 5.5 dB on top of the 5 dB insertion loss, due to the increase of PDL and the Gaussian response. Similar behaviour was measured for all other coarse channels.

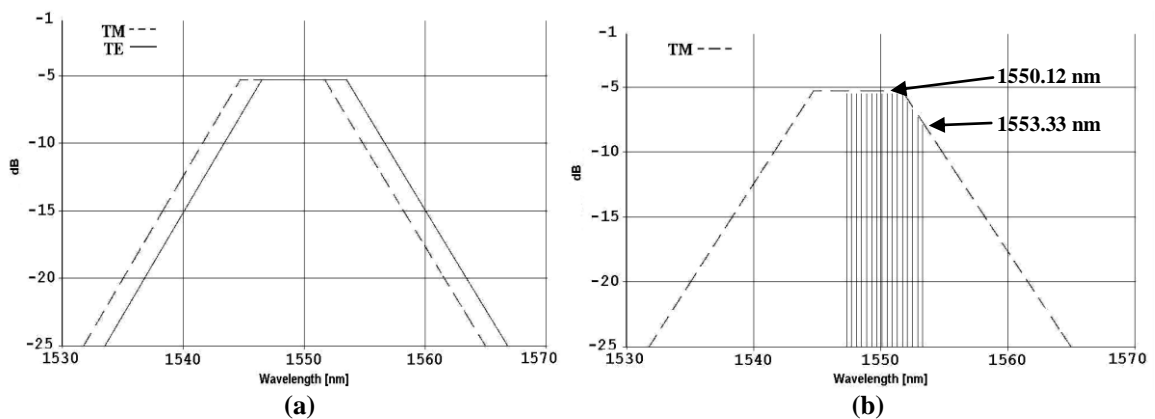


Figure 4-9 Polarisation-dependent wavelength shift of central flat-top channel

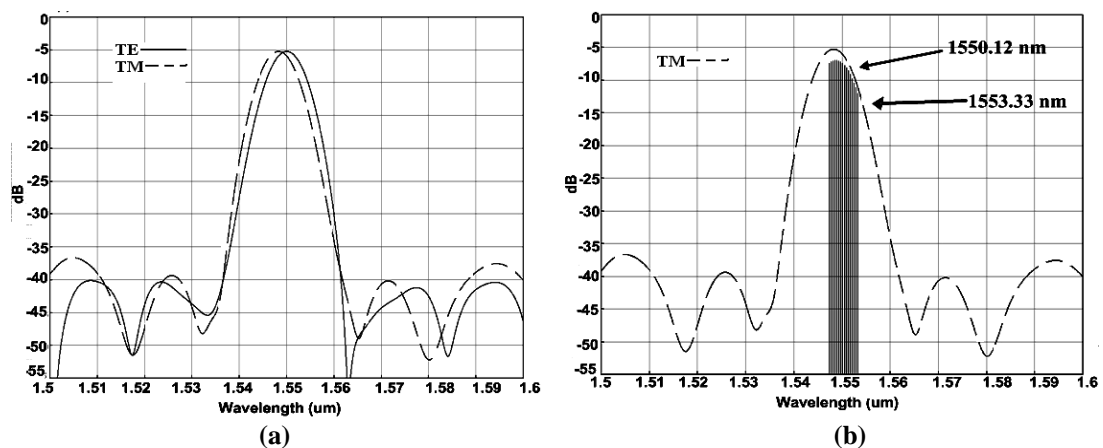


Figure 4-10 Polarisation-dependent wavelength shift of central Gaussian channel

To investigate variation in channel loss with respect to the power distribution among TE and TM modes depending on the applied wavelength SOP, the three wavelengths at $\lambda_2^1=1553.33$, $\lambda_2^9=1550.12$ nm and $\lambda_2^{16}=1547.32$ nm, corresponding to the longest, centre and shortest wavelength of coarse channel $\lambda_2=1550$ nm, were utilised. Consequently, a polarisation controller was employed in the system simulator to control the SOP of each wavelength at the input port of either the Gaussian or flat AWG and an optical power meter, applied at the AWG output port, was employed for power measurements. The entire Poincaré sphere was scanned by varying the azimuth ψ and ellipticity X between -90° to 90° and -45° to 45° respectively in steps of 10° in order to map the entire 1550 nm channel.

The Gaussian channel mapping for the longest wavelength at 1553.33 nm is shown in Figure 4-11(a), exhibiting optical loss in the range of 7.5 dB for azimuth and ellipticity at 0° , and 10.5 dB for azimuth and ellipticity at 90° and 0° respectively. Figure 4-11(b), representing the centre wavelength at 1550.12 nm, follows similar trend, nevertheless with optical loss in the range of 5 dB to 5.7 dB. Alternatively, Figure 4-11(c), representing the shortest wavelength at 1547.32 nm, exhibits a complementary curve with optical loss in the range of 5.4 dB and 6.8 dB, confirming the imbalance between both parts of the passband, due to shifting

On the contrary, the flat-top channel mapping for longest wavelength is shown in Figure 4-11(d), exhibiting optical loss in the range of 5.2 dB for azimuth and ellipticity at 0° , and 7.2 dB for azimuth and ellipticity at 90° and 0° respectively. Nevertheless, Figure 4-11(e) and Figure 4-11(f), representing the centre and shortest wavelengths respectively, exhibit loss of 5 dB across the entire Poincaré due to 0 dB PDL.

Results indicate that since the Gaussian channel does not maintain the same trend across the entire passband and does not apply identical loss characteristics for all wavelengths in the

passband, there is no preferred SOP to allow minimum channel loss for all wavelengths. On the contrary, the flat-top channel provides minimum loss characteristics by employing wavelengths with azimuth and ellipticity both at 0° .

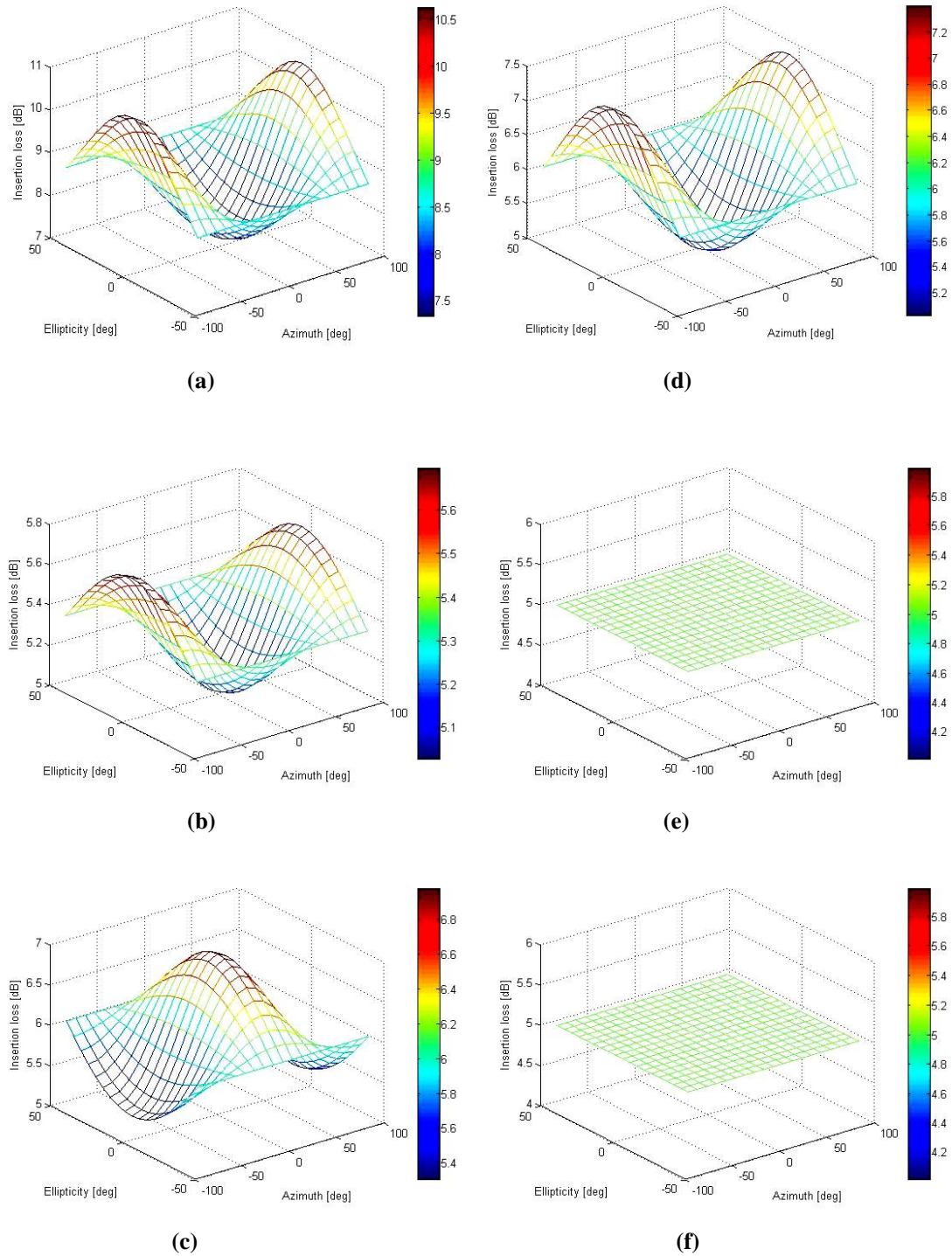


Figure 4-11 Insertion loss versus wavelength state of polarisation
Gaussian channel (a) $\lambda_2^1 = 1553.33$ nm (b) $\lambda_2^9 = 1550.12$ nm (c) $\lambda_2^{16} = 1547.32$ nm
Flat-top channel (d) $\lambda_2^1 = 1553.33$ nm (e) $\lambda_2^9 = 1550.12$ nm (f) $\lambda_2^{16} = 1547.32$ nm

Since the PDW shift in the AWG is caused by birefringence in the device waveguides and as a result the signal routed via the TM response travels at different speed with respect to its TE counterpart, the potential of PMD to limit the network bidirectional data rates was investigated. In that direction, the TM standard AWG module of the Gaussian coarse AWG model was reconfigured by modifying its parameter normalized propagation constant β . In that sense, the parameter β was set 0.66, as opposed to its TE counterpart 0.6, that was calculated from the effective index contrast Δn [31], i.e. birefringence 0.003 of the prototype AWG [3].

Subsequently, the amount of time delay between the two waveguide transmitted modes was recorded by applying an optical signal modulated by a sine-wave in both the TE and TM modes. Figure 4-12 demonstrates the time-delay at the output port of the AWG for which, as expected, the TM mode lags by a figure of approximately 14 ps with respect to its TE equivalent.

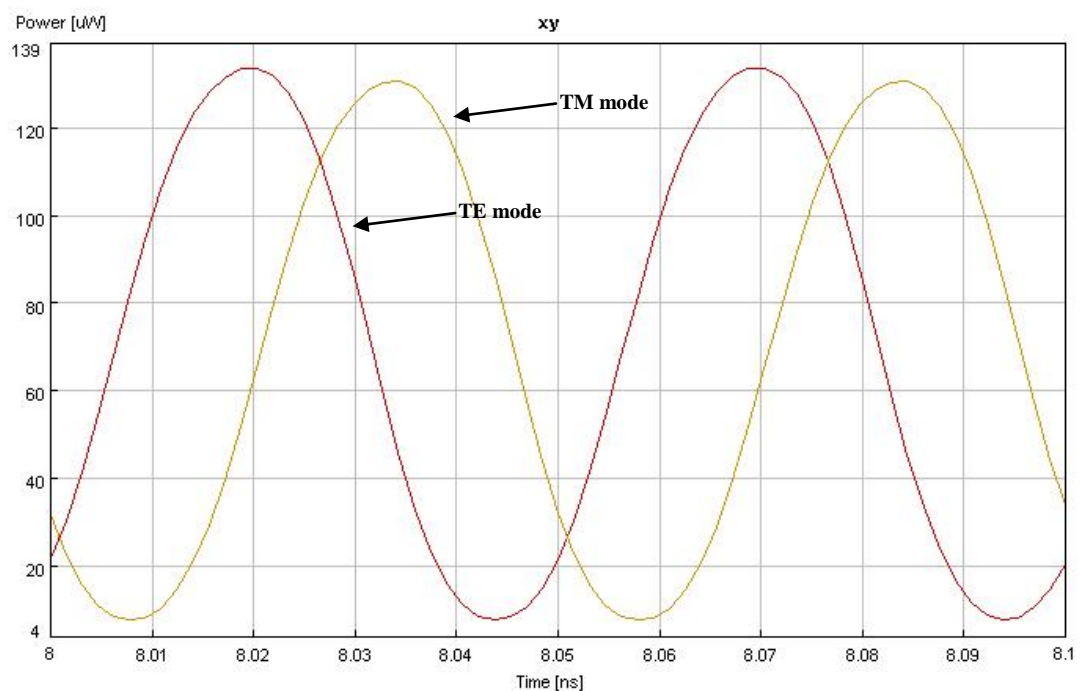


Figure 4-12 Time-delay between the AWG TE and TM modes due to PMD

To evaluate the effect of such a time-delay figure between the two transmitted modes on the network downstream and upstream transmissions, BER responses are drawn in Figure 4-13 for the centre wavelength at 2.5 Gbit/s, 10 Gbit/s and 20 Gbit/s to represent the standard, next generation and beyond, maximum data rates. Consequently, BER plots confirm error-free transmission at all modulation speeds with measured BERs of 10^{-9} , at a maximum 1.1 dB penalty at 20 Gbit/s due to PMD induced both in the AWG and SSMF. Further analysis for 2.5 Gbit/s and 10 Gbit/s data rates, demonstrates no penalty in BER between employing either the reconfigured or original AWGs, suggesting that the AWG PMD figure of 14 ps does not impose any limitation at these data rates. Nevertheless, at 20 Gbit/s transmission rate, by excluding the SSMF in order to evaluate the contribution of the AWG solely, a moderate penalty of 0.5 dB can be observed due to the device PMD, consequently demonstrating equal contribution of penalty as for the 20 km SSMF PMD.

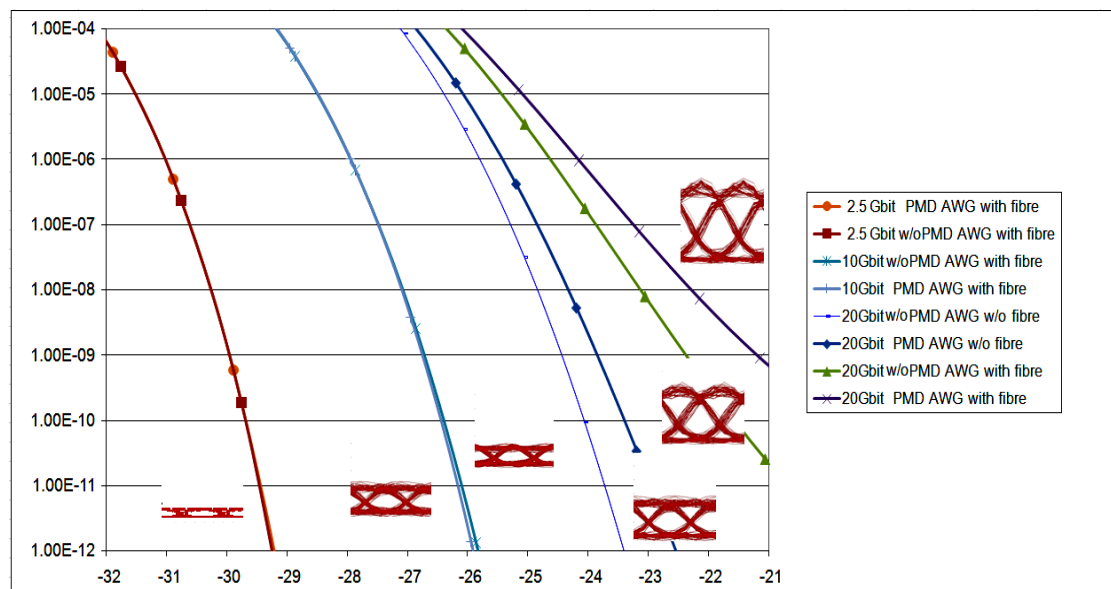


Figure 4-13 Measured BER for downstream and upstream when accounting for the PMD in the AWG

4.5 Power budget and transmission evaluation

The network is designed for power budget and insertion loss of the components in the optical path to allow error-free transmission of all wavelengths of a PON. Analysis of power budget measurements are summarised in Table 4-7.

Table 4-7 Network power budget

Parameter	Value
DFB average launched power	2 dBm
MZM insertion loss	5 dB
Optical circulator	1 dB
Coarse AWG loss	10.5 dB @ WDM PON 5.7 dB @ TDM PON
20 km SSMF loss	4 dB
distribution point losses	5.5 dB @ WDM PON 12.5 dB @ TDM PON
Optical circulator	1 dB
APD sensitivity @ 10^{-9} BER	-29.25 dBm

According to Table 4-7 the highest link loss of 27 dB for a WDM-PON was measured for the longest wavelength including the losses of a MZM, Gaussian AWG, distribution point multiplexer, 20 km SSMF and two optical circulators, caused mainly by the coarse AWG due to the Gaussian response and PDL. In the case for a TDM-PON the highest link loss of 29.2 dB, consists of the losses of a MZM, coarse AWG, 20 km SSMF, 1:16 distribution point optical splitter and 2 optical circulators.

Unlike in the WDM scenario for which the AWG insertion loss reaches up to 10.5 dB, the AWG insertion loss in the TDM case does not exceed 5.7 dB, since the transmitted wavelength is naturally positioned at the centre of the AWG coarse channel, consequently compensating the significant loss of the passive optical splitter in the distribution point. The benefit of the

WDM-PON over TDM-PON arises when each PON accommodates 32 ONUs. Consequently, the link loss in the WDM scenario does not vary due a key feature of AWGs, for which increasing the device channel number does not affect the its insertion loss, while in the scenario of TDM supporting 32 ONUs, a 1:32 passive optical splitter will result in approximately additional 3 dB loss.

To evaluate the network bidirectional performance, BER curves were drawn for the longest wavelengths at $\lambda_2^1=1553.33$ nm and $\lambda_4^1=1592.52$ nm of the coarse channels $\lambda_2=1550$ nm and $\lambda_4=1590$ nm respectively as shown in Figure 4-14. In that sense the best and worst case scenario coarse channels in the middle and boundaries of the device FSR and the highly attenuated wavelengths within, were investigated. Results confirm error free transmission with measured BER of 10^{-9} at -29.5 dBm receiver sensitivity for both upstream and downstream with no more than 0.5 dB penalty between the longest wavelengths due to the AWG routing across the device FSR.

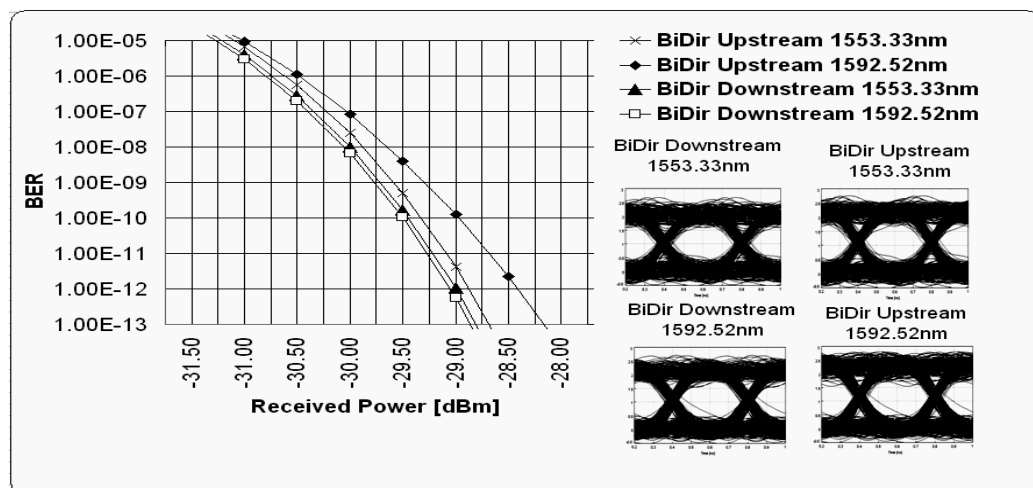


Figure 4-14 Measured BER for upstream and downstream transmission

4.6 Summary

This chapter presented an innovative access network architecture utilising the coarse channels of a Gaussian AWG in the OLT to demonstrate high scalability and interoperability among TDM and WDM PONs through a single OLT with coarse-fine grooming.

Simulation results for upstream and downstream routing have indicated that 7 nm-wide passband windows of the AWG enabled all ONUs representing each physical PON to be multiplexed through coarse ITU-T grid channels to a common destination in the OLT demonstrating the potential of the proposed architecture to handle multiple PONs concurrently using a single tunable laser through a single AWG router device [27], potentially allowing for smooth network upgrade from standard TDM to forthcoming multiwavelength PONs and efficient management of bandwidth among various physical PONs.

The chapter further investigated the effect the PDW shift on the accurate routing of all ONUs comprising a PON. The Gaussian passband window of the devised AWG exhibited no more than 3 dB PDL incurred on the transmitted wavelengths due to a worst case PDW shift of 1.8 nm [3] and worst case device phase errors of 270° [30]. In contrast, the passband window of the flat AWG demonstrated 0 dB PDL for most of the transmission band and reached to a maximum of 2.5 dB for similar shifting figures. Investigation for the variation of AWG channel loss versus the SOP of the transmitted wavelength reported losses in the range of 5 dB to 10.5 dB for the Gaussian channel and 5 dB to 7.2 dB for the flat channel. In addition, no preferred SOP to maintain minimum loss for all wavelengths was demonstrated for the Gaussian channel due to the imbalance in the passband operation, while linear horizontal SOP may be applied to all wavelengths of the flat channel to maintain minimum channel loss.

Finally, BER analysis for the network bidirectional transmission demonstrated error-free performance with achieved rates of 10^{-9} at -29.5 dBm receiver sensitivity and 0.5 dB maximum power variation between the coarse channels. In addition, PMD in the AWG was shown not to impose limitation of the network bidirectional transmission when data rates of up to 20 Gbit/s are employed. The ability of a single OLT accessing in downstream various physical PONs with multiple wavelengths allows centralised bandwidth allocation according to subscriber service levels and smooth migration path between time-shared and densely-penetrated access networks.

4.7 References

- [1] Y. Shachaf, C.-H. Chang, P. Kourtessis, and J. M. Senior, "Multi-PON access network using a coarse AWG for smooth migration from TDM to WDM PON," *OSA Optics Express*, vol. 15, pp. 7840-7844, 2007.
- [2] ITU-T Recommendation: G.694.2, "Spectral Grids for WDM Applications: CWDM wavelength grid," 2003.
- [3] J. Jiang, C. L. Callender, C. Blanchetière, J. P. Noad, S. Chen, J. Ballato, and J. Dennis W. Smith, "Arrayed Waveguide Gratings Based on Perfluorocyclobutane Polymers for CWDM Applications," *IEEE Photonics Technology Letters*, vol. 18, pp. 370-372, 2006.
- [4] C. Chang-Joon and O. Nam-Hyun, "WDM/TDM PON system employing a wavelength-selective filter and a continuous-wave shared light source," *IEEE Photonics Technology Letters*, vol. 10, pp. 1325-1327, 1998.
- [5] S.-J. Park, C.-H. Lee, K.-T. Jeong, H.-J. Park, J.-G. Ahn, and K.-H. Song, "Fiber-to-the-Home Services Based on Wavelength-Division-Multiplexing Passive Optical Network (Invited)," *IEEE/OSA Journal of Lightwave Technology*, vol. 22, pp. 2582-2591, 2004.
- [6] I. Tsalamanis, E. Rochat, and S. D. Walker, "Experimental demonstration of cascaded AWG access network featuring bi-directional transmission and polarization multiplexing," *OSA Optics Express*, vol. 12, pp. 764-769, 2004.
- [7] Y. Shachaf, P. Kourtessis, and J. M. Senior, "An interoperable access network based on CWDM-routed PONs," presented at 33rd European Conference and Exhibition on Optical Communication (ECOC), Berlin, Germany, 2007.
- [8] Furukawa Electric Co Ltd,
["http://www.furukawa.co.jp/fitel/eng/active/pdf/Cooled/ODC-4R001B_FOL15TCWA-Axx.pdf,"](http://www.furukawa.co.jp/fitel/eng/active/pdf/Cooled/ODC-4R001B_FOL15TCWA-Axx.pdf) 2005.

- [9] ITU-T Recommendation G.984.2, "Gigabit-capable passive optical networks (GPON): Physical media dependent (PMD) layer specification," 2003.
- [10] ITU-T Recommendation G.984.3, "Gigabit-capable passive optical networks (GPON): transmission convergence layer specification," 2003.
- [11] ITU-T Recommendation G.984.1, "Gigabit-capable Passive Optical Networks (GPON): General characteristics," 2003.
- [12] ITU-T Recommendation G.984.3, "Gigabit-capable passive optical networks (GPON): transmission convergence layer specification," 2003.
- [13] Fujitsu, "<http://www.fujitsu.com/downloads/OPTCMP/lineup/10gln/10glnsingle-catalog-e.pdf>," 2005.
- [14] Alliance Fiber Optic Products Inc (AFOP), "<http://www.afop.com/pdf/products/Micro%20Optics/Optical%20Circulators/Optical%20Circulator.pdf>," 2004.
- [15] JDSU, "<http://www.jdsu.com/products/optical-communications/products/detectors-receivers.html>," 2007.
- [16] K. Inoue, "Influence of fiber four-wave mixing in multichannel return-to-zero (RZ) signal transmissions," *IEEE Photonics Technology Letters*, vol. 8, pp. 293-295, 1996.
- [17] "<http://www.vpi Photonics.com/>," VPI Photonics Inc., 2007.
- [18] K.-D. Langer, K. Habel, F. Raub, and M. Seimetz, "CWDM access network and prospects for introduction of full-duplex wavelength channels," presented at Conference on Networks & Optical Communications (NOC 2005), UCL, 2005.
- [19] Corning Incorporated. NY, "<http://www.vinkarola.com/pdf/Corning%20SMF-28e%20Fiber.pdf>," 2007.

- [20] W. Fischer, "Fiber to the Home Deployments in Europe-Architectural and Technological," presented at Conference on Networks & Optical Communications (NOC 2005), UCL, London, 2005.
- [21] W. Lee, M. Y. Park, S. H. Cho, J. Lee, C. Kim, G. Jeong, and B. W. Kim, "Bidirectional WDM-PON Based on Gain-Saturated Reflective Semiconductor Optical Amplifiers," *IEEE Photonics Technology Lett.*, vol. 17, pp. 2460-2462, 2005.
- [22] A. Banerjee, Y. Park, F. Clarke, H. Song, S. Yang, G. Kramer, K. Kim, and B. Mukherjee, "Wavelength-division-multiplexed passive optical network (WDM-PON) technologies for broadband access: a review [Invited]," *OSA Journal of Optical Networking*, vol. 4, pp. 737-758, 2005.
- [23] C.-H. Lee, S.-M. Lee, K.-M. Choi, J.-H. Moon, S.-G. Mun, K.-T. Jeong, J. H. Kim, and B. Kim, "WDM-PON experiences in Korea [Invited]," *OSA Journal of Optical Networking*, vol. 6, pp. 451-464, 2007.
- [24] J.-H. AHN, H.-J. LEE, W.-Y. HWANG, M.-C. OH, M.-H. LEE, S. G. HAN, H.-G. KIM, and C. H. YIM, "Polymeric 1x16 Arrayed Waveguide Grating Multiplexer Using Fluorinated Poly (Arylene Ethers) at 1550 nm," *IEICE Transactions on Communications*, vol. E82, pp. 406-408, 1999.
- [25] ANDevices Inc., "<http://www.andevices.com/PDF/APMUX1050.pdf>," 2007.
- [26] Spectrolab, "[http://www.spectrolab.com/Datasheets/APD/OE APD 2-5G Die.pdf](http://www.spectrolab.com/Datasheets/APD/OE_APD_2-5G_Die.pdf)," 2003.
- [27] Y. Shachaf, P. Kourtessis, and J. M. Senior, "Multiple - PON access network architecture," presented at IEEE/IET 2nd International Access Technologies (ICAT), Cambridge, UK, 2006.
- [28] R. M. Craig, "Accurate Spectral Characterization of Polarization-Dependent Loss," *IEEE/OSA Journal of Lightwave Technology*, vol. 21, pp. 432-437, 2003.

- [29] T. Goh, S. Suzuki, and A. Sugita, "Estimation of waveguide phase error in silica-based waveguides," *IEEE/OSA Journal of Lightwave Technology*, vol. 15, pp. 2107-2113, 1997.
- [30] A. Wang, "Private communication." Fremont, CA: ANDevices, Inc, 2006.
- [31] "Photonics Modules Reference Manual," VPIcomponentMaker, VPIphotonics Inc., 2007.